Unveiling the Link between Airy-like Self-Acceleration and Diametric Drive Acceleration

Ping Zhang,[1] Yi Hu,[1,*] Domenico Bongiovanni,[1,2] Zhili Li,[1] Roberto Morandotti,[2,3] Zhigang Chen,[1,4] and Jingjun Xu[1,†]

[1]*Key Laboratory of Weak-Light Nonlinear Photonics, Ministry of Education, School of Physics, Nankai University, Tianjin 300071, China*
[2]*INRS-EMT, 1650 Boulevard Lionel-Boulet, Varennes, Quebec J3X 1S2, Canada*
[3]*Institute of Fundamental and Frontier Sciences, University of Electronic Science and Technology of China, Chengdu 610054, China*
[4]*Department of Physics and Astronomy, San Francisco State University, San Francisco, California 94132, USA*

We theoretically reveal the link between two types of self-acceleration mechanisms widely emerging in wave dynamics and experimentally demonstrate such a connection via pulse interactions in nonlinear optical fibers. We find that, in order to realize a pulse pair subjected to a diametric drive acceleration, one of the two components can be directly obtained from a self-accelerating Airy-like pulse under appropriate conditions. Such a form of synchronized acceleration cannot be achieved by approaches previously used to generate diametric drive acceleration. Our results generalize the fundamental concept of diametric drive acceleration and may bring about unconventional approaches to control self-accelerating waves.

It is common knowledge that acceleration originates from an applied external force. A notable exception is an Airy wave packet undergoing a self-accelerating propagation in the absence of an external potential. Discovered initially in the realm of quantum mechanics [1], self-accelerating Airy waves were later revealed ubiquitously in various physical systems of wave dynamics [2–12]. In particular, self-accelerating optical waves [2,3] have received a great amount of attention, mainly triggered by their peculiar characteristics and potential applications [4] such as in optical manipulation [13,14], imaging, and microscopy [15–17], as well as nonlinear optics [18–22]. In principle, the intrinsic acceleration is associated with a semi-infinite structure of the wave profiles, consisting of an intense main lobe and numerous auxiliary sublobes. The energy stored in the sublobes continuously flows toward the main lobe region, leading to the main lobe acceleration. This mechanism extends to nonlinear self-accelerating wave packets [18,23,24], also featuring semi-infinite profiles.

Well before the discovery of Airy wave packets, another kind of self-accelerating behavior, named "runaway motion," was proposed in general relativity [25]. Essentially, it describes a counterintuitive movement of two mutually interacting objects with opposite mass signs, where an object with negative inertial mass would be expected to accelerate in the opposite direction to an exerted force: As a consequence, one object chases the other, but meanwhile the other tends to escape. Without resorting to any external force, they can jointly accelerate solely via their mutual interactions, arousing many intriguing ideas toward fuel-free propulsion [26] or the interpretation of mysterious cosmological phenomena [27]. Such captivating dynamics were recently introduced in optics, by realizing coacceleration of two optical pulses (typically a soliton pulse and a dispersive pulse) driven by their nonlinear interactions [28,29]. This so-called diametric drive acceleration was also actively pursued in the optical spatial domain [30–33] as well as in Bose-Einstein condensates [34].

Although the two different kinds of self-acceleration mentioned above have been investigated in the past, their connection, to the best of our knowledge, has never been explored. In this Letter, we propose and demonstrate unified self-acceleration in the context of pulse interaction in nonlinear optical fibers. We find that, in order to generate a pair of pulses subject to diametric drive acceleration, the dispersive pulse can be obtained from an Airy-like profile through truncation. Our analytical prediction is directly verified by experimental observation, realizing the coacceleration of a truncated Airy pulse and a soliton pulse. We emphasize that, here, we do not propose yet another demonstration of diametric drive acceleration, but rather we develop a scheme that generalizes the concept of wave acceleration, paving the way to novel and unexplored applications of self-accelerating waves.

To design an optical diametric drive acceleration in optical fibers, two coupled nonlinear Schrödinger equations are required [28]:

$$i\frac{\partial A}{\partial z} = \frac{\beta_{2A}}{2}\frac{\partial^2 A}{\partial \tau^2} - f_A(|A|^2, |B|^2)A$$

$$i\frac{\partial B}{\partial z} = \frac{\beta_{2B}}{2}\frac{\partial^2 B}{\partial \tau^2} - f_B(|A|^2, |B|^2)B, \qquad (1)$$

where A and B are the electric field envelopes of two pulses representing the soliton and the dispersive pulse, respectively, z is the propagation distance, τ is time in the retarded frame, β_{2A} (β_{2B}) is the anomalous (normal) group-velocity dispersion coefficient, and $f_{A,B}(|A|^2, |B|^2)$ represents the nonlinear term. It is worth noting that Eq. (1) has similar forms in other physical systems [34]. Specifically, in the model studied here, $f_A(|A|^2, |B|^2) = \gamma_A(|A|^2 + 2|B|^2)$ and $f_B(|A|^2, |B|^2) = \gamma_B(|B|^2 + 2|A|^2)$, where the coefficients γ_A and γ_B indicate the nonlinear strength, while the first and second terms in the nonlinear functions describe self-phase modulation (SPM) and cross-phase modulation (XPM) [35], respectively. In the analysis that follows, we adopt the same fiber parameters used in our experimental setting: $\beta_{2A} = -1.3 \times 10^{-3}$ ps$^2 \cdot$ m^{-1}, $\beta_{2B} = 1.2 \times 10^{-3}$ ps$^2 \cdot$ m^{-1}, and $\gamma_A = \gamma_B = 0.5 \times 10^{-3}$ W$^{-1} \cdot$ m^{-1}. Under these conditions, the pulse A (B) experiences a self-focusing (-defocusing) nonlinearity. In the absence of pulse A, pulse B can be endowed with self-acceleration solely via the Airy mechanism [2,18]. The resulting nonlinear accelerating mode shows a similar profile to the linear Airy counterpart [Fig. 1(a)], relying on its semi-infinite profile to guarantee a persistent acceleration [18]. Once a truncation is imposed on the Airy wave packet [i.e., by letting $B(\tau > 0) = 0$], the truncated Airy wave accelerates only for a limited range of distances [Fig. 1(b)]. Now, we add pulse A (shaped as a hyperbolic-secant soliton) to replace the removed sublobes [Fig. 1(c)]. Because of XPM, we expect that the soliton is

attracted by the truncated Airy-like pulse, which, on the other hand, is repelled by the soliton. This is due to the fact that the two pulses have opposite dispersions, akin to opposite masses in a diametric drive acceleration [28,29]. Provided that the nonlinearly induced acceleration properly matches the Airy-like acceleration (characterized by g), the two pulses experience a runaway motion [Fig. 1(c)], as described by the following equations:

$$\left\langle A(\tau)\left|\frac{\partial f_A}{\partial \tau}\right|A(\tau)\right\rangle = -\frac{gI_A}{\beta_{2A}},$$

$$\left\langle B(\tau)\left|\frac{\partial f_B}{\partial \tau}\right|B(\tau)\right\rangle = -\frac{gI_B}{\beta_{2B}}, \qquad (2)$$

where I_A and I_B are the soliton and dispersive pulse energies, respectively, while the left term accounts for the "force" reciprocally experienced by each pulse. Using Eq. (2), we readily determine the soliton with the desired peak power and temporal location (see Supplemental Material [36]). A detailed comparison between the three evolutions in Figs. 1(a)–1(c) is further performed by placing the Airy-like pulses in the accelerating reference frame (defined by $s = \tau - gz^2/2$). When examining the input and output temporal profiles as shown in Figs. 1(d)–1(f), one can clearly see that the soliton effectively replaces the truncated part of the Airy-like solution, thus maintaining the acceleration. When the soliton is not present, a finite-energy Airy-like pulse always experiences decay due to the truncation and, thus, cannot preserve a long dispersion-free propagation (see more simulations in Supplemental Material [36]).

To form a coaccelerating pair via our proposed scheme, overlapping between the two pulses is required. However, the ensuing XPM may actually reshape the truncated Airy-like pulse due to the fact that the sublobes eliminated in the truncation cannot be exactly replaced by the soliton, consequently unbalancing the relationship between the force and the target acceleration in Eq. (2). To quantify this effect, the temporal deflection of the truncated Airy-like pulse subjected to a diametric drive acceleration is compared with the ideal case (i.e., $\delta_\tau = gz^2/2$). For this purpose, we define the parameter $\Delta = (\delta'_\tau - \delta_\tau)/|\delta_\tau| \times 100\%$, where δ'_τ is the numerically calculated temporal change of the pulse "centroid" (i.e., $\int_{-\infty}^{+\infty}|B|^2\tau d\tau / \int_{-\infty}^{+\infty}|B|^2 d\tau$) at a certain propagation distance. The values of Δ for Airy-like pulses with different parameters, at the output after a 4-km-long propagation, are presented in Fig. 2. The detrimental influence of the XPM term can be reduced by employing an intense peak power (characterized by P_B) or a sufficiently large number (defined by n) of pulse lobes.

In order to relate the interaction force with the target acceleration, different truncated Airy-like pulses can be paired with solitons featuring different parameters. Following Newton's third law, the energies of the two
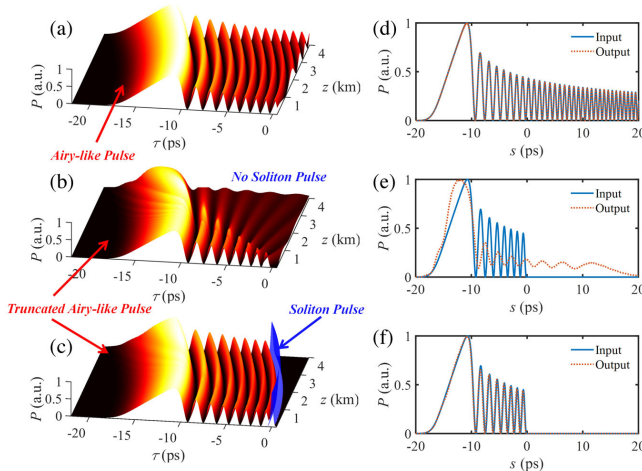

FIG. 1. Numerical evolution of a nonlinear Airy-like pulse under three different initial conditions: (a) without and (b),(c) with truncation of the sublobes. In (c), a pairing soliton pulse is also injected. (d)–(f) Input and output profiles of the Airy-like pulse corresponding to (a)–(c), in an accelerating reference frame.
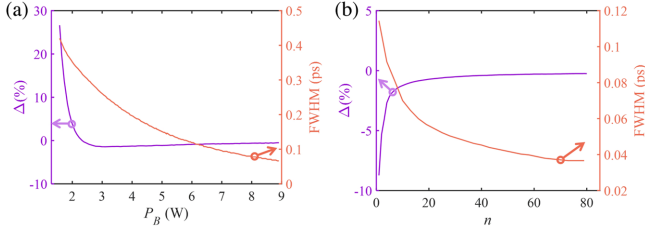
FIG. 2. Characterization on the acceleration deviation of a truncated Airy-like pulse when paired with a soliton and the temporal range at which the two pulses overlap for different (a) peak powers and (b) lobe numbers in the truncated Airy-like pulse. In (a), $n = 8$; in (b), $P_B = 4$.
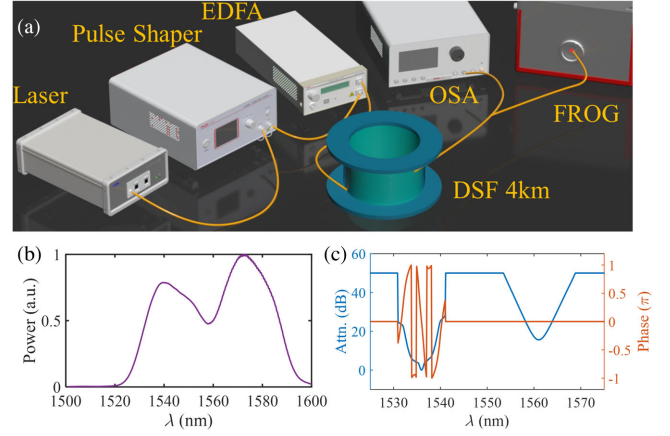

FIG. 3. (a) Experimental setup; (b) spectrum of the laser source; (c) typical spectral amplitude and wrapped phase modulations uploaded in the pulse shaper for generating the target pulses.

pulses satisfy the relation $(gI_A/\gamma_A\beta_{2A}) = -(gI_B/\gamma_B\beta_{2B})$ that is readily obtained from Eq. (2), hence showing a proportional relationship. Thus, for truncated Airy-like pulses featuring higher energies (obtained, i.e., by increasing either the peak power or the lobe number), one can deduce that the pairing soliton has a narrower temporal width (a parameter inversely proportional to the soliton energy [35]). Consequently, the overlapping region of the two pulses tends to be shorter at high pulse energies, thus weakening the adverse effect coming from XPM. To verify this, the force distribution applied on the truncated Airy-like pulse, which acquires the form of $|B|^2(\partial f_B/\partial\tau)$, is analyzed at the input by calculating its full width at half maximum to characterize the effective interaction range. As expected, this range decreases as the peak power or the number of lobes in the truncated Airy-like pulse increases (Fig. 2).

To corroborate the validity of the proposed scheme, we further carry out experiments using the setup schematically illustrated in Fig. 3(a). A dispersion-shifted fiber (DSF, 4 km long) with the zero-dispersion wavelength at 1547.7 nm is employed for pulse propagation. The pairing soliton and the Airy-like pulses are obtained by reshaping a femtosecond pulse featuring a broadband spectrum [Fig. 3(b)] via a programmable pulse shaper [Fig. 3(c)]. Their center wavelengths are selected to be 1561 and 1536 nm, not only to impart a self-focusing and -defocusing nonlinear evolution, respectively, but also to prompt the same group velocity (in order to avoid walk-off effects). Additionally, a linear phase is applied to the spectrum of the Airy-like pulse in order to adjust the delay between the two pulses. Before injection into the fiber, the pulse powers are properly amplified by an erbium-doped fiber amplifier (EDFA). At the fiber output, an optical spectrum analyzer (OSA) and a frequency-resolved optical gating (FROG) system are employed to measure the spectral and the temporal profiles, respectively.

Since other optical effects are routinely present in fibers, we consider in our model also the third-order dispersion (TOD) and the linear loss (characterized by β_3 and α, respectively) so as to provide a better reproduction of the

experimental pulse evolution in simulations. In this case, the coupled propagating equations are modified as

$$i\frac{\partial A}{\partial z} = \frac{\beta_{2A}}{2}\frac{\partial^2 A}{\partial\tau^2} + i\frac{\beta_3}{6}\frac{\partial^3 A}{\partial\tau^3} - \gamma_A(|A|^2 + 2|B|^2)A + \frac{i\alpha}{2}A$$
$$i\frac{\partial B}{\partial z} = \frac{\beta_{2B}}{2}\frac{\partial^2 B}{\partial\tau^2} + i\frac{\beta_3}{6}\frac{\partial^3 B}{\partial\tau^3} - \gamma_B(|B|^2 + 2|A|^2)B + \frac{i\alpha}{2}B.$$
$$(3)$$

Dispersion terms of orders higher than TOD as well as higher-order nonlinear effects can be neglected by employing input pulses of large duration. In our fiber, $\beta_3 = 1 \times 10^{-4}$ ps$^3 \cdot$m^{-1} and $\alpha = 0.33$ dB/km, representing the small influence exerted by both TOD and loss. In the first demonstration, we use a truncated Airy-like pulse with $n = 3$ and $P_B = 2.3$ W. In simulation, this pulse exhibits an expected acceleration when paired with the designed soliton, even in the presence of both TOD and loss [Fig. 4(a)], while its spectrum shows a quasilinear redshift [Fig. 4(b)]. In contrast, the soliton tends to move to a shorter wavelength. Although the TOD can help an Airy-like pulse propagating alone to be resistant to dispersion [37], our scheme featuring soliton control is more advantageous in terms of keeping dispersion-free evolutions (see more simulations in Supplemental Material [36]). In our experiment, the input pulses are generated based on the simulations. After a nonlinear interaction in the fiber, the two pulses nearly preserve their original profiles at the output [Fig. 4(c)], with some slight changes in pulse width that are mainly caused by loss of power. Note that, for a better comparison with the numerical results, the measured outputs have been artificially imposed with a temporal offset that cannot be measured with our FROG technique. Looking at the spectral domain, the two pulses undergo inverted frequency shifts [Fig. 4(d)], which represents a distinctive experimental signature of their coacceleration
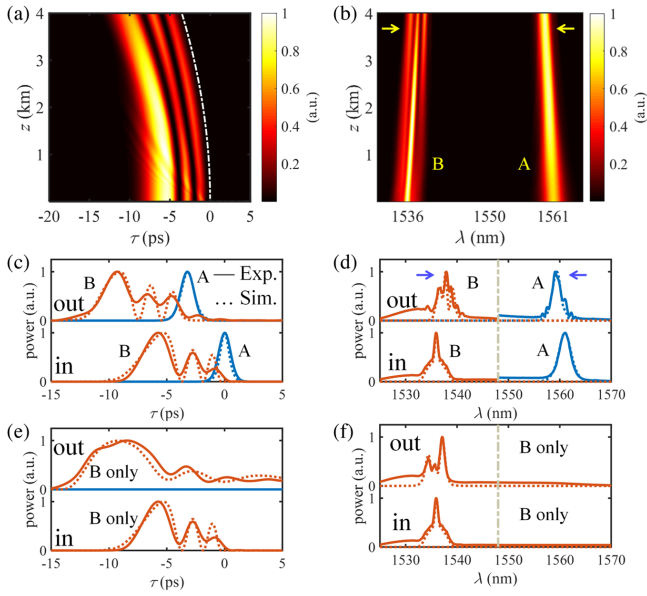
FIG. 4. Experimental and numerical results of a diametric drive acceleration involving a truncated Airy-like pulse with three lobes and a soliton pulse. (a),(b) Simulations depicting (a) the temporal evolution of the Airy-like pulse extracted from the jointly accelerating pair (whose designed spatiotemporal path is plotted by the dash-dotted line) and (b) the related spectral evolution of both pulses. (c),(d) Measured (solid lines) and numerically calculated (dotted lines) input and output (c) temporal profiles and (d) spectra for the diametric drive acceleration. (e),(f) The same as (c),(d), for the case where the truncated Airy-like pulse propagates alone. Note that all results in each panel are presented in a normalized form.
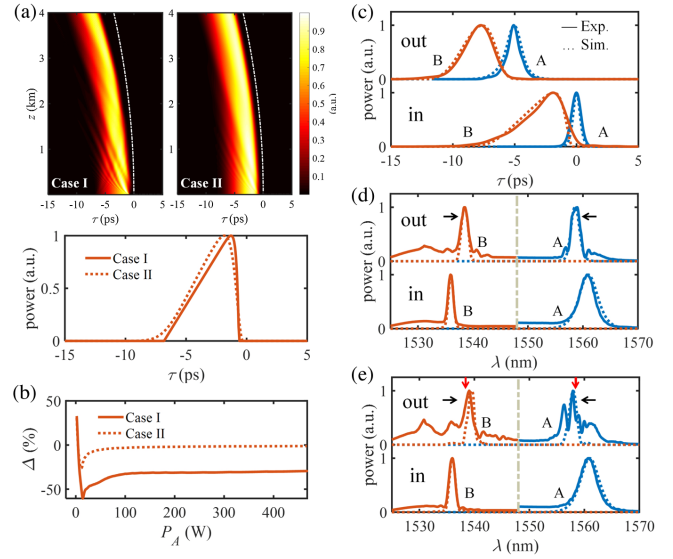

FIG. 5. Comparison between diametric drive accelerations realized via the conventional method (case I) and our approach (case II). (a) Temporal evolutions (upper panel) of the dispersive pulses (whose inputs are shown in the bottom panel) extracted from the paired propagations and expected along the path plotted by the dash-dotted lines; (b) numerical pulse acceleration deviations for different soliton peak powers. Note that both TOD and loss are not considered in (a) and (b). (c)–(e) Measurements (solid lines) and corresponding numerical simulations (dotted lines) of the input and output temporal (c) and spectral (d),(e) profiles of the paired pulses in cases II (c),(d) and I (e). The vertical arrows in (e) mark the spectral peak locations of the outputs in (d).

during nonlinear propagation. Based on the good agreement between numerical and experimental results, we can conclude that the acceleration of the truncated Airy-like pulse is maintained via the mechanism of diametric drive acceleration. It should be pointed out that, when the pairing soliton is absent, the truncated pulse can no longer preserve its shape, and, instead, it becomes much wider under a self-defocusing nonlinearity [Fig. 4(e)]. Meanwhile, its output spectrum [Fig. 4(f)] nearly resides at the original position, experiencing a broadening caused by SPM. Furthermore, when we attempt to include more lobes for the Airy-like pulse, we find that the generation and detection of complex pulses become more difficult mainly due to the limited resolution of both pulse shaper and FROG.

By trimming off all the sublobes of the Airy-like pulse, so as to leave the main lobe only, the diametric drive acceleration studied here reduces to the conventional case where the dispersive pulse has only one peak. Next, we compare our approach with that reported in Ref. [28] for designing the single-peak dispersive pulse. The main difference is that the dispersion is considered in our scheme, in contrast to the approach in Ref. [28]. As such, the pulse acceleration realized in that early method exhibits an evident deviation from the desired spatiotemporal path

[Fig. 5(a)]. A detailed characterization (by the coefficient Δ as defined before) of the acceleration deviation is presented in Fig. 5(b). One can notice that the diametric drive pair designed by neglecting the dispersion always shows a larger acceleration with respect to the desired behavior, even at high pulse energies where the value of Δ for our case approaches zero. We further investigate, experimentally, the difference between the two methods. Without loss of generality, we fix the peak power of the soliton pulse to be 19.5 W. First, we realize the diametric drive acceleration via our approach. A good agreement with the simulation based on Eq. (3) is shown in Figs. 5(c) and 5(d), and similar features in terms of pulse shape preservation and inverted frequency shifts are observed as in the case in Fig. 4. Second, while keeping the other conditions unchanged, the dispersive pulse is replaced by the one engineered without considering the dispersion. In this latter case, both spectra for the paired pulses undergo a larger shift [Fig. 5(e)], given that the actual pulse propagation experiences a larger acceleration compared with our case.

In conclusion, we have analytically proposed and experimentally demonstrated the connection between two types of widely studied optical wave acceleration, the Airy-like acceleration and the diametric drive acceleration, using nonlinear fiber optics as our test bench. We found that one

component of a diametrically driving pair can be directly obtained from a truncated Airy-like wave packet, and this finding is more evident at the high-energy regime for the paired pulses. Our results generalize the concept of diametric drive acceleration and, even more importantly, bring about a more precise way to control wave acceleration in general. Besides the optical applications proposed with the conventional diametric drive acceleration [28,29], there are some operations unique to our approach, where the number of lobes in the Airy-like pulse can be properly controlled. For instance, Airy-like pulses with different numbers of lobes may be employed as different symbols to encode information, which can provide alternative coding schemes (different from binary coding; see Ref. [38]) for transmitting information with enhanced data-carrying capacity. Beyond the field of optics, our approach can be directly extended to the systems governed by the nonlinear Schrödinger equation where dispersions with opposite signs coexist, such as in acoustic and water waves [39,40]. Furthermore, for the systems described by the Dirac equation, our results may trigger the investigation of unifying self-accelerating waves [41] and the runaway motion [25]. This unification not only is of fundamental interest, but may also bring about new possibilities to control the wave dynamics in various Dirac materials [42].

[*] yihu@nankai.edu.cn
[†] jjxu@nankai.edu.cn

[1] M. V. Berry and N. L. Balazs, Am. J. Phys. **47**, 264 (1979).
[2] G. A. Siviloglou, J. Broky, A. Dogariu, and D. N. Christodoulides, Phys. Rev. Lett. **99**, 213901 (2007).
[3] G. A. Siviloglou and D. N. Christodoulides, Opt. Lett. **32**, 979 (2007).
[4] N. K. Efremidis, Z. Chen, M. Segev, and D. N. Christodoulides, Optica **6**, 686 (2019).
[5] A. Chong, W. H. Renninger, D. N. Christodoulides, and F. W. Wise, Nat. Photonics **4**, 103 (2010).
[6] P. Zhang, S. Wang, Y. Liu, X. Yin, C. Lu, Z. Chen, and X. Zhang, Opt. Lett. **36**, 3191 (2011).
[7] L. Li, T. Li, S. M. Wang, C. Zhang, and S. N. Zhu, Phys. Rev. Lett. **107**, 126804 (2011).
[8] A. Minovich, A. E. Klein, N. Janunts, T. Pertsch, D. N. Neshev, and Y. S. Kivshar, Phys. Rev. Lett. **107**, 116802 (2011).
[9] N. Voloch-Bloch, Y. Lereah, Y. Lilach, A. Gover, and A. Arie, Nature (London) **494**, 331 (2013).
[10] P. Zhang, T. Li, J. Zhu, X. Zhu, S. Yang, Y. Wang, X. Yin, and X. Zhang, Nat. Commun. **5**, 4316 (2014).
[11] U. Bar-Ziv, A. Postan, and M. Segev, Phys. Rev. B **92**, 100301(R) (2015).
[12] S. Fu, Y. Tsur, J. Zhou, L. Shemer, and A. Arie, Phys. Rev. Lett. **115**, 034501 (2015).
[13] J. Baumgartl, M. Mazilu, and K. Dholakia, Nat. Photonics **2**, 675 (2008).
[14] R. Schley, I. Kaminer, E. Greenfield, R. Bekenstein, Y. Lumer, and M. Segev, Nat. Commun. **5**, 5189 (2014).
[15] S. Jia, J. C. Vaughan, and X. Zhuang, Nat. Photonics **8**, 302 (2014).
[16] T. Vettenburg, H. I. C. Dalgarno, J. Nylk, C. Coll-Lladó, D. E. K. Ferrier, T. Čižmár, F. J. Gunn-Moore, and K. Dholakia, Nat. Methods **11**, 541 (2014).
[17] J. Wang, X. Hua, C. Guo, W. Liu, and S. Jia, Optica **7**, 790 (2020).
[18] I. Kaminer, M. Segev, and D. N. Christodoulides, Phys. Rev. Lett. **106**, 213903 (2011).
[19] P. Polynkin, M. Kolesik, J. V. Moloney, G. A. Siviloglou, and D. N. Christodoulides, Science **324**, 229 (2009).
[20] M. Henstridge, C. Pfeiffer, D. Wang, A. Boltasseva, V. M. Shalaev, A. Grbic, and R. Merlin, Science **362**, 439 (2018).
[21] P. Jia, Z. Li, Y. Hu, Z. Chen, and J. Xu, Phys. Rev. Lett. **123**, 234101 (2019).
[22] T. Ellenbogen, N. Voloch-Bloch, A. Ganany-Padowicz, and A. Arie, Nat. Photonics **3**, 395 (2009).
[23] A. Lotti, D. Faccio, A. Couairon, D. G. Papazoglou, P. Panagiotopoulos, D. Abdollahpour, and S. Tzortzakis, Phys. Rev. A **84**, 021807(R) (2011).
[24] Y. Hu, Z. Sun, D. Bongiovanni, D. Song, C. Lou, J. Xu, Z. Chen, and R. Morandotti, Opt. Lett. **37**, 3201 (2012).
[25] H. Bondi, Rev. Mod. Phys. **29**, 423 (1957).
[26] M. G. Millis, J. Propuls. Power **13**, 577 (1997).
[27] J. S. Farnes, Astron. Astrophys. **620**, A92 (2018).
[28] S. Batz and U. Peschel, Phys. Rev. Lett. **110**, 193901 (2013).
[29] M. Wimmer, A. Regensburger, C. Bersch, M.-A. Miri, S. Batz, G. Onishchukov, D. N. Christodoulides, and U. Peschel, Nat. Phys. **9**, 780 (2013).
[30] Y. Pei, Y. Hu, C. Lou, D. Song, L. Tang, J. Xu, and Z. Chen, Opt. Lett. **43**, 118 (2018).
[31] Y. Pei, Y. Hu, P. Zhang, C. Zhang, C. Lou, C. E. Rüter, D. Kip, D. Christodoulides, Z. Chen, and J. Xu, Opt. Lett. **44**, 5949 (2019).
[32] Y. Pei, Z. Wang, Y. Hu, C. Lou, Z. Chen, and J. Xu, Opt. Lett. **45**, 3175 (2020).
[33] A. Alberucci, C. P. Jisha, U. Peschel, and S. Nolte, Phys. Rev. A **100**, 011802(R) (2019).
[34] H. Sakaguchi and B. A. Malomed, Phys. Rev. E **99**, 022216 (2019).
[35] G. P. Agrawal, *Nonlinear Fiber Optics* (Springer, New York, 2000).
[36] See Supplemental Material at http://link.aps.org/supplemental/10.1103/PhysRevLett.127.083901 for the method to design diametric drive acceleration and additional simulations.

[37] I. M. Besieris and A. M. Shaarawi, Phys. Rev. E **78**, 046605 (2008).

[38] F. Mitschke, *A Brief History of Fiber-Optic Soliton Transmission* (Springer, Singapore, 2018).

[39] S. Fu, J. Zhou, Y. Li, L. Shemer, and A. Arie, Phys. Rev. Lett. **118**, 144501 (2017).

[40] M. Kurosu, D. Hatanaka, and H. Yamaguchi, Phys. Rev. Applied **13**, 014056 (2020).

[41] I. Kaminer, J. Nemirovsky, M. Rechtsman, R. Bekenstein, and M. Segev, Nat. Phys. **11**, 261 (2015).

[42] M. Polini, F. Guinea, M. Lewenstein, H. C. Manoharan, and V. Pellegrini, Nat. Nanotechnol. **8**, 625 (2013).